Fusion Engineering and Design 122 (2017) 356–364

Contents lists available at ScienceDirect

Fusion Engineering and Design

journal homepage: www.elsevier.com/locate/fusengdes

The DTT device: Power supplies and electrical distribution system

Alessandro Lampasi[a,*], Pietro Zito[a], Fabio Starace[a], Pietro Costa[a], Giuseppe Maffia[a], Simone Minucci[b], Elena Gaio[c], Vanni Toigo[c], Loris Zanotto[c], Sergio Ciattaglia[d]

[a] National Agency for New Technologies, Energy and Sustainable Economic Development (ENEA), Frascati, Italy
[b] University of Naples Federico II, Naples, Italy
[c] Consorzio RFX, Padua, Italy
[d] EUROfusion Consortium, Garching, Germany

HIGHLIGHTS

- This paper presents the power supply and electrical systems of the Divertor Tokamak Test (DTT) facility.
- The analysis includes at least 30 superconducting coils, about 120 MW for the additional heating systems and almost 100 MW for the auxiliary services.
- The voltage, current and power ratings were estimated moving from a reference scenario.
- The 100-MVA permanent load can exceed 400 MVA with a duty cycle of 100 s/3600s.
- The analysis includes at least 30 superconducting coils and more than 200 MW for the additional and auxiliary systems.

ARTICLE INFO

Article history:
Received 30 July 2016
Received in revised form
18 December 2016
Accepted 22 January 2017
Available online 4 February 2017

Keywords:
Divertor Tokamak Test (DTT)
Power supply
AC/DC converter
Inverter
Switching network unit (SNU)
Fast discharge unit (FDU)
Quench protection
High power delivery

ABSTRACT

This paper presents the design criteria and the preliminary characteristics of the power supply and electrical systems of the Divertor Tokamak Test (DTT) facility. The power supply system has to feed: 6 superconducting modules of the central solenoid, 6 poloidal field superconducting coils, 18 toroidal field superconducting coils designed for a current up to 50 kA, some coils for plasma fast control and vertical stabilization, the electron (ECRH) and ion (ICRH) cyclotron additional heating systems designed to deliver about 25 MW to the plasma, further 20 MW to the plasma generated by a neutral beam injector (NBI) and all the auxiliary systems and services.

The analysis was carried out on a reference scenario with a plasma current of 6 MA, mainly to estimate the electrical power needed to operate the facility, but also to identify some design choices and component ratings.

1. Introduction

The management of the heat exhaust is one of the most challenging problems for the realization of fusion energy. The European roadmap proposes a Divertor Tokamak Test (DTT) facility to address such a problem [1]. This facility is conceived as a test bed mainly for alternative solutions (as divertor magnetic configurations and liquid metals) able to solve the power exhaust problem in DEMO-relevant integrated plasma scenarios. However, in the present proposal, DTT will be a complete tokamak that requires comprehensive power supply (PS) and electrical systems able to feed the magnetic field coils, the additional heating systems and the auxiliary services [2–7].

Fig. 1 shows an overview of the DTT plasma configuration and main coils. The coil positions and cross-sections were designed with an iterative procedure taking into account the plasma specifications as well as the geometrical and financial constraints [8–10]. The overall optimization included the type of superconductors and the number of turns in each coil [11], looking for the best trade-off between the current per turn and the PS voltage. The preliminary analysis of the required PS ratings presented in this paper was necessary also to assesses the feasibility of the selected DTT configuration and design.

The DTT PS system has to feed (see also Fig. 1):

* Corresponding author.
E-mail address: alessandro.lampasi@enea.it (A. Lampasi).

http://dx.doi.org/10.1016/j.fusengdes.2017.01.036

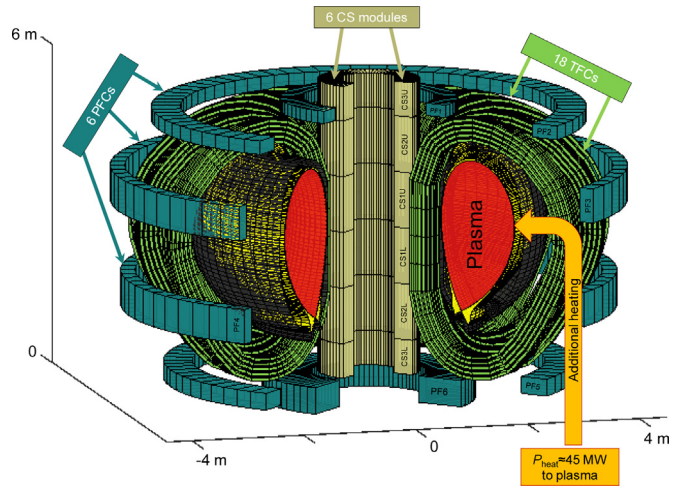

Fig. 1. 3-D view of the DTT coil and plasma shape during a typical single null configuration. Besides the main coils emphasized in the figure, further internal coils (as IC5 and IC6) will be used for plasma control and stabilization.

- The central solenoid (CS) divided in 6 superconducting modules (CS3U, CS2U, CS1U, CS1L, CS2L, CS3L), each having an independent PS circuit;
- 6 poloidal field superconducting coils (PFCs), classified as PF1, PF2, PF3, PF4, PF5, PF6.
- 18 toroidal field superconducting coils (TFCs), designed to operate with a current up to 50 kA.
- Some fast plasma control coils, including at least two non-superconducting internal coils (IC5 and IC6) for plasma vertical stabilization.
- The electron (ECRH) and ion (ICRH) cyclotron additional heating (and current drive) systems, designed to deliver an effective power of about 25 MW to the plasma [12,13].
- All the auxiliary systems and services.
- An upgrade of the heating system, able to deliver further 20 MW to the plasma, especially by a neutral beam injector (NBI) [12,14].

This paper presents the conceptual design and the preliminary characteristics of the DTT PSs and electrical systems. The analysis was carried out mainly to estimate the electrical power needed to operate the facility and to identify some design choices and component ratings.

The calculations were performed on a reference single null scenario (plasma current), that is expected to be the most demanding one in terms of electrical power and stress on the components, as a snowflake configuration is not achievable at the DTT maximum plasma current (I_p = 6 MA) [9]. The experiment duty cycle for this scenario is expected to be 100s/3600s.

Due to the importance of realizing the DTT scopes respecting the time schedule and budget constraints [10], the general principle for the preliminary design was to identify and select solutions ensuring a good technological feasibility confidence. Some promising alternative solutions or improvements have already been identified and will be investigated in parallel with the main project.

The voltages and currents to be provided by the coil PSs were estimated by applying the current time-evolution in each coil (known in the reference scenario) to the magnetically coupled circuits model and taking into account the switching network unit (SNU) contributions [15]. Because of the geometrical position of the coils and their consequent mutual magnetic coupling, the CS, PFC and IC powers must be estimated together, whilst the other contributions can be considered as rather independent.

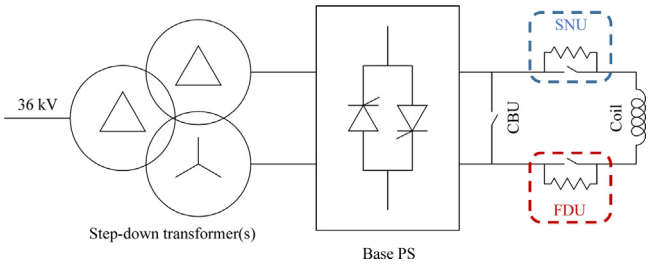

Fig. 2. General scheme of a CS or PFC PS circuit.

Even if the heating systems will be upgraded in successive phases [12], the power contribution related to the additional heating systems was estimated for the maximum expected peak value.

At the present stage of the project, there are not good enough details to model some contributions, such as the power supply systems to control the error fields or the magnetohydrodynamic (MHD) instabilities. Moreover, the control of the local magnetic configuration close to the divertor target will be obtained by a special set of internal coils [8,9]. However, the experience gained on other tokamaks teaches that the involved power levels have a limited impact on the overall ratings and requirements [16].

For this reason and for other model approximations, but also in order to allow modifications and future upgrades, a reasonable increment is applied to the results of the power estimation.

2. Poloidal power supply systems

2.1. Circuital configurations

The PS system of each CS and PF circuit consists of:

1 A step-down transformer (from medium voltage at 36 kV to low voltage below 1 kV) optimized to supply the downstream converters. Due to the need to obtain 12-pulse operations, the transformer could be implemented either by two secondary windings or by splitting it in two separated transformers.
2 A Base PS containing at least two AC/DC converters based on thyristor bridges. The two converters operate with a 30° phase displacement to obtain a 12-pulse waveform. As shown in Fig. 2, each switch is composed of two back-to-back thyristors to implement 4-quadrant operations [17].
3 A crowbar unit (CBU) to by-pass the Base PS and the load in case of fault [18].
4 A commutation system, that is a SNU in most of the cases or a simple by-pass switch (BPS) for the PF3 and PF4 coils.
5 A fast discharge unit (FDU) able to insert a resistor in the circuit when it is necessary to discharge the magnetic energy stored in the load coil (especially for superconducting quench protection) [19].

2.2. SNUs, FDUs and BPSs

Since the Base PSs are not able to produce the abrupt current derivative required to initiate and sustain the plasma breakdown, a SNU is inserted in each CS and PFC circuit. This general scheme is valid for all the CS and PF coils, with the exception of the PF3 and PF4 coils, as they have a BPS instead of the SNU that is closed after the plasma breakdown.

Both the SNUs and the FDUs are based on fast switching of high DC currents. Good performances and repeatability are expected thanks to the idea of using a hybrid switch already explored for JT-60SA [15,19]. The inadequate velocity and repeatability of the main electromechanical BPS is virtually hidden by some parallel elec-

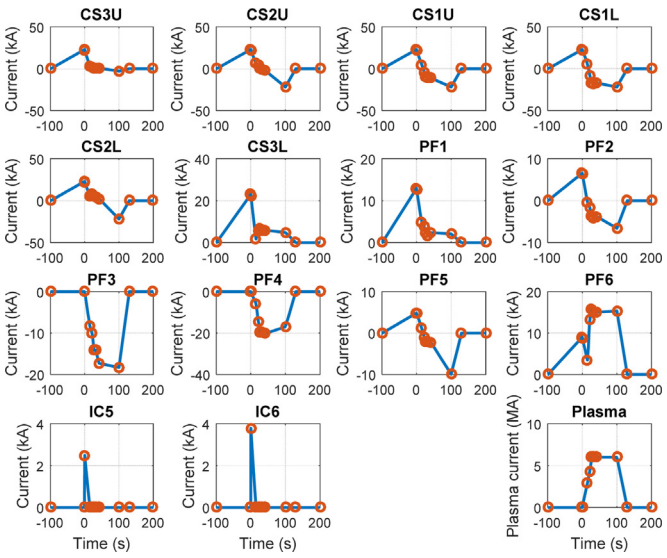

Fig. 3. Reference current scenario for the CS, poloidal and internal coils and for the plasma. The circles represent the 12 defined time instants.

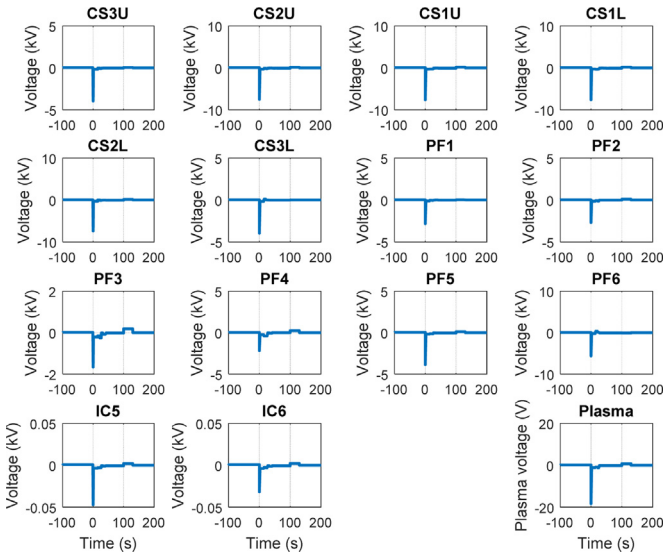

Fig. 4. Coil and plasma voltages for the current reference scenario in Fig. 3.

tronic static devices. The same devices improve the expected BPS lifecycle and reliability by limiting the arc phenomena [20]. However, the SNUs and the FDUs have different functions and required performances. For instance, a SNU needs to perform two successive operations (opening and closing sequences) in every plasma experiment, whilst a FDU is opened to discharges the magnetic energy only in case of fault.

The values of the SNU resistances and of the consequent breakdown voltages are identified with the procedure presented in next section. The obtained values are feasible and quite homogenous.

2.3. Coil functional models and numerical results

The design moved from a reference scenario defined in terms of time evolution of the coil currents to estimate successively the coil voltages, the Base PS voltages and the active and reactive powers. The numerical data are based on the 6 MA reference scenario that is the most demanding one in terms of electrical power. The currents in this scenario are shown in Fig. 3.

The profiles reported in Fig. 3 for the IC5 and IC6 currents are only examples, as they actually depend on the plasma evolution. More pulses with the same shapes are expected in the practical cases. While this have a limited impact in terms of power, the presented curves are useful to assess the PS current and voltage ratings.

The DTT experiments are described by the current scenarios, consisting in the profiles of the coil currents versus time for each supplied poloidal coil (6 CS modules, 6 PF coils, 2 ICs). The solution of the MHD equations provides also the behavior of plasma current for the given scenarios.

Therefore, a current scenario is fully characterized by a time-dependent column vector $\underline{I}(t)$ with dimension 15 (14 coils and the plasma) including at least the current samples for the N time instants t_1, t_2, …, t_n, …, t_N when the currents are defined. The values of $\underline{I}(t)$ are emphasized as red circles in Fig. 3 for the reference scenario with $N = 12$. Even though the scenario is defined by few samples, the waveforms are oversampled for a better numerical approximation. The first 14 rows of $\underline{I}(t)$ gives the vector $\underline{I}_{\text{coil}}(t)$ of the currents flowing in the 14 coils, the last row contains the plasma current $I_{\text{p}}(t)$.

The magnetic interactions among the elements of the tokamak poloidal cross-section are characterized by a square and symmetric 15×15 inductance matrix $\underline{\underline{M}}$. This matrix contains at least the mutual inductances among the supplied (active) coils and between them and the plasma current. A more refined model should include the parameters of the "passive" elements of the tokamak in the matrix $\underline{\underline{M}}$. The lack of these parameters at this stage is expected to be compensated by the safety margins introduced in the final results.

The entries in the main diagonal of $\underline{\underline{M}}$ correspond to the self-inductance of each coil and range from 78 mH to 154 mH for the CS modules, attaining the maximum value of about 340 mH for PF4.

Analogously to $\underline{I}_{\text{coil}}(t)$, it is possible to define a voltage vector $\underline{V}_{\text{coil}}(t)$ having dimension 14 containing the time evolution of the voltage across the two terminals of each of the 14 coils when the scenario currents flow through them. A further column vector $\underline{V}(t)$ with dimension 15 can be obtained by adding the plasma loop voltage in the last row. Hence, the $\underline{V}(t)$ corresponding to a current scenario $\underline{I}(t)$ can be calculated by applying the formula:

$$\underline{v}(t) = \underline{\underline{M}} \frac{d\underline{I}(t)}{dt} \tag{1}$$

Fig. 4 shows the voltages across the two terminals of the coils and for the plasma loop for the current scenario shown in Fig. 3.

2.4. Average models and results for the PS systems

The voltage across the coil terminals $\underline{V}_{\text{coil}}(t)$ is simply given by the first 14 rows of $\underline{V}(t)$. The actual average voltage $\underline{V}_{\text{PS}}(t)$ to be produced by the PS systems should account also for the voltage drops in the circuit (DC bus bars, cryogenic transitions, connections, joints, parasitic effects, SNUs and so on):

$$\underline{v}_{\text{PS}}(t) = \underline{v}_{\text{coil}}(t) + \left(R_{\text{drop}} + \underline{r}_{\text{SNU}}(t)\right) \underline{I}_{\text{coil}}(t) \tag{2}$$

where $\underline{r}_{\text{SNU}}(t)$ is the SNU resistance, that is not constant during the scenario, and $\underline{R}_{\text{drop}}$ includes all the other resistances in series with the load coil, that can be assumed constant for the present analysis. Moreover, the small resistances of the superconducting coils can be neglected.

The voltage present across the PF3 and PF4 terminals during the breakdown phase is the voltage induced by the currents in the other coils.

For each circuit containing a SNU, the corresponding row of $\underline{V}_{\text{PS}}(t)$ is the voltage to be produced by the Base PS during the whole scenario except in the breakdown phase, whilst the volt-

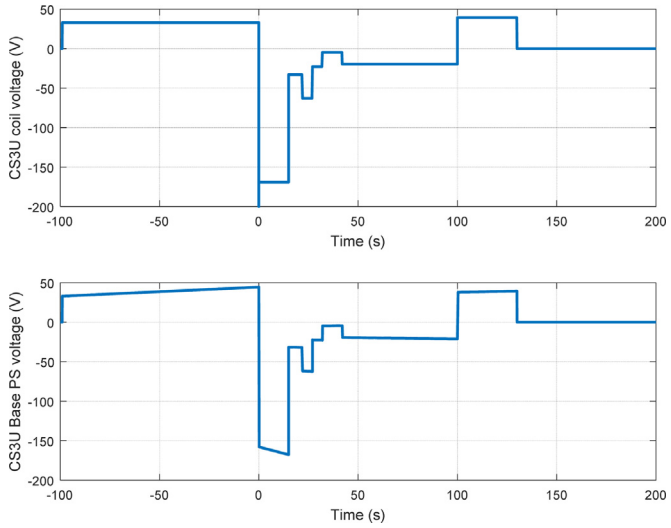

Fig. 5. Comparison between the voltage across the coil terminals (hiding a part of the negative peak at almost 4 kV) and the voltage to be produced by the Base PS for the CS3U module.

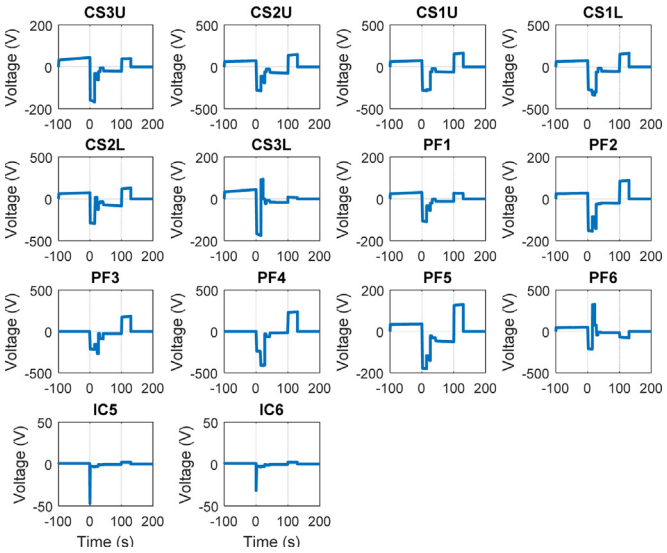

Fig. 6. Voltage to be produced by each Base PS to achieve the current scenario in Fig. 3.

age at the breakdown depends also on the lumped resistance R_{SNU} inserted by the SNU. Such resistance is a degree of freedom in the PS design. Moving from the criterion of minimizing the PS power, the minimum SNU resistance can be calculated and selected.

The voltage at the SNU terminals has to raise quickly and with low jitter. The SNU opening time is practically instantaneous in the model. Thus, the ideal R_{SNU} for each circuit can be calculated from the voltage variation at the breakdown divided by the available coil current:

$$R_{SNU} = \frac{V_{PS}(0) - V_{PS}(\Delta t_0)}{I_{coil}(0)} \tag{3}$$

where Δt_0 is a minimal time interval after the conventional time zero given by the breakdown initiation. Normally, several resistance values can be selectable in a SNU. The value obtained by (3) for the maximum PS current provides a reference for the minimum SNU resistance (in the order of hundreds of milliohms for the considered scenario).

For sake of clearness, the difference between V_{PS} and V_{coil} is shown in Fig. 5 for the case of the CS3U module. For a better comparison, the figure does not show the negative peak at almost 4 kV that is expected across the CS3U coil (as visible in Fig. 4).

The voltage curves in Fig. 6 take into account also the circuit drops and the SNU effects, then they represent the voltage to be generated by each Base PS. The semiconductors and the other bridge components, as well as the step-down transformers, are selected to comply with these values.

2.5. Power scenarios

The instantaneous power generated by the Base PS

$$p_{PS}(t) = v_{PS}(t) \cdot i_{PS}(t) \tag{4}$$

practically corresponds to the instantaneous active power $P(t)$ absorbed from the grid through the step-down transformers. A small part of this power (about 2%) is dissipated in the connections, in the transformers and in the thyristor junctions.

The thyristor bridges can sustain high powers with good reliability but require high reactive power $Q(t)$ to operate. This can be estimated by approximated formulae reported in the technical literature [21,22].

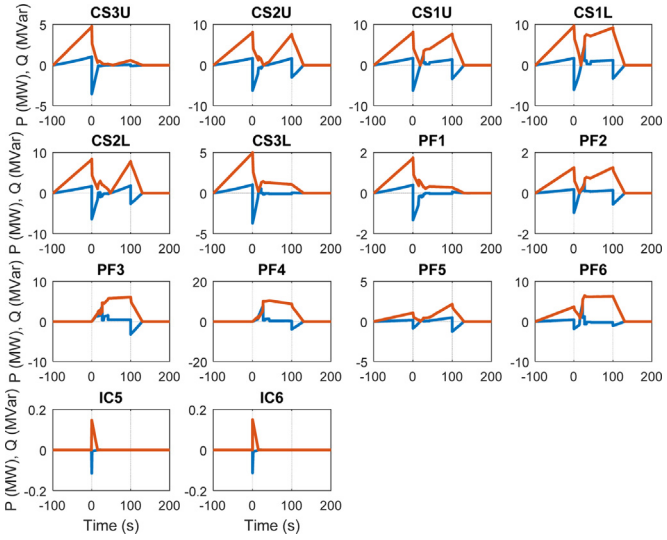

Fig. 7. Active (blue curves) and reactive (red curves) powers for each coil PS producing the reference scenario. (For interpretation of the references to colour in this figure legend, the reader is referred to the web version of this article.)

The active and reactive power scenarios for each coil are shown in Fig. 7. These powers are necessary to produce the current in Fig. 3 with the voltage in Fig. 6.

The impact of the PS systems on the distribution network can be quantified by the apparent power $S(t)$ that is the module of the complex power

$$\vec{S}(t) = P(t) + jQ(t) \tag{5}$$

The weight of the active and reactive powers is normally quantified by the power factor

$$\cos\varphi = \frac{P}{S} \tag{6}$$

The total power contribution of the CS, PF and IC PS systems is summarized in Fig. 8. While $P(t)$ has a positive peak of 20 MW, $Q(t)$ can reach peaks up to 60 MVar leading to similar values for $S(t)$.

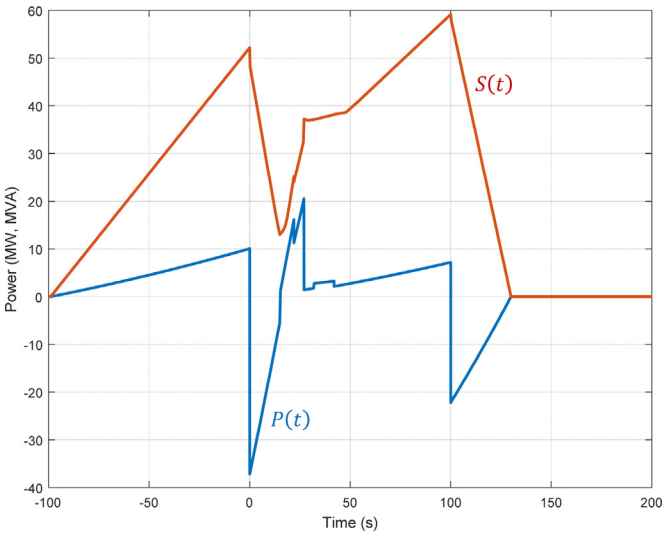

Fig. 8. Total active and apparent power for the CS, PF and IC PS systems.

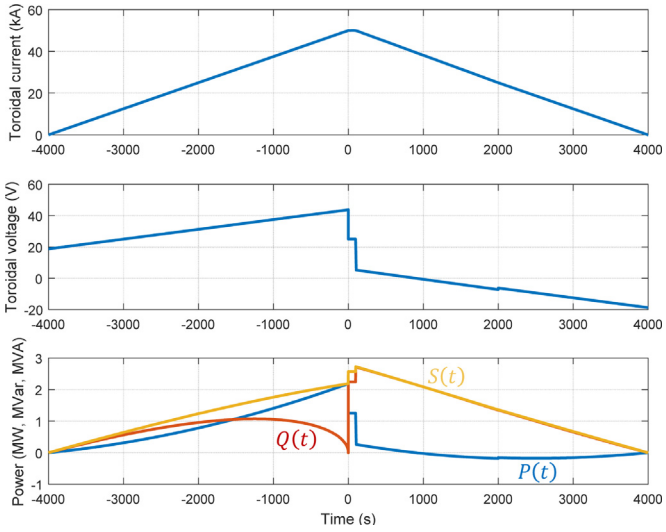

Fig. 9. TFC current, voltage and electric powers when the coils are charged and discharged for a single 100 s experiment.

3. Power supplies for the toroidal field coils

The TFC PS system is designed to provide the required DC current to the superconducting coils for an entire experimental period (hours or days). The total coil inductance is about 1.5 H. The flat-top current of 50 kA can be attained by applying a relatively low voltage for a long time. Afterwards, the obtained flat-top current can be maintained for many plasma experiments.

Just to illustrate the involved parameters, Fig. 9 presents a reference situation where the coils are charged and discharged for a single 100 s experiment. The resulting powers are quite low, if compared with the values shown in Fig. 8, that are instead characterized by a duty cycle of 100s/3600s. In practice, thanks to the limited values and variations, the TFC power contribution can be taken into account by including it in the auxiliary power described in Section 5.

Since the TFC operations do not require a SNU, only the Base PS controls the voltage. However, some FDUs in series are foreseen to protect groups of TFCs [23]. A polarity changer is being planned to be inserted between the TFC current feeders.

Table 1
Assumed approximated performances of the additional heating systems considered for the DTT electrical design.

Additional heating system	Power P_{heat}	Efficiency η	Power factor cosφ
ICRH	10 MW	60%	0.7
ECRH	15 MW	30%	0.9
P-NBI	0	40%	0.6
N-NBI	20 MW	25%	0.6
Global equivalent	45 MW	35%	0.65

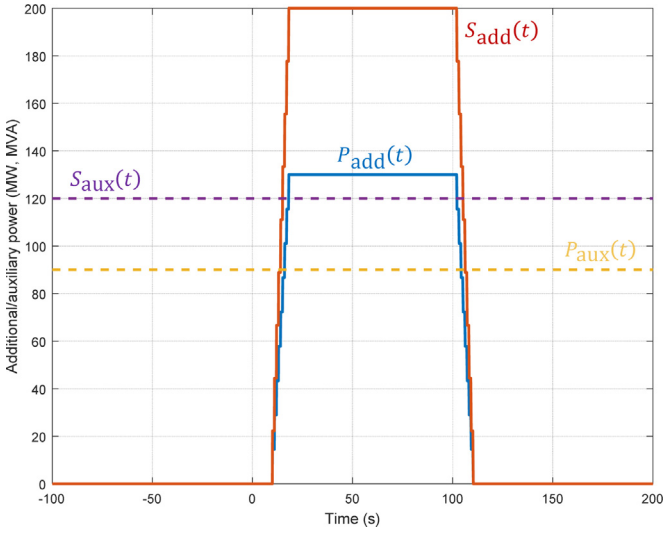

Fig. 10. Power contributions from the additional heating and auxiliary systems.

4. Power supplies for additional heating

Even if the additional heating systems will be upgraded in successive phases, their power contribution has been estimated assuming a total power of 45 MW coupled to the plasma for 100s/3600s [12].

The actual electrical power required to obtain such heating effect on the plasma depends on the adopted system. In fact, the heating power P_{heat} delivered to the plasma is a fraction of the additional electrical power P_{add} absorbed from the grid, depending on the efficiency η of the specific heating system:

$$P_{heat}(t) = \eta \cdot P_{add}(t) = \eta \cdot S_{add}(t) \cdot \cos\varphi \quad (7)$$

In the first phase of DTT, a mix of ICRH Ion Cyclotron (klystrons or tetrodes at 60–90 MHz) and ECRH (gyrotrons at 170 GHz) are considered, as indicated by the first two rows in Table 1, while NBI is the most probable way to upgrade the power (N-NBI due to the high beam energy required to heat the plasma center). The approximate performances of such systems are summarized in Table 1, where some worst-case assumptions and safety margins are introduced. The efficiency considered in the table is the percentage of the active power absorbed from the distribution network that is actually delivered to the plasma.

Considering a mix of additional heating systems upgradable in the future, the pessimistic values $\eta = 35\%$ and $\cos\varphi = 0.65$ are assumed in the last row of Table 1 as the global equivalent efficiency and power factor, respectively.

As shown in Fig. 10, a realistic scenario is assumed for the evolution of the heating power during the experiment: after the breakdown, the power delivered to the plasma (P_{heat}) is increased with steps of 5 MW/s. Accordingly, the electrical power absorbed from the grid (P_{add}) is increased with steps of about 14 MW/s up

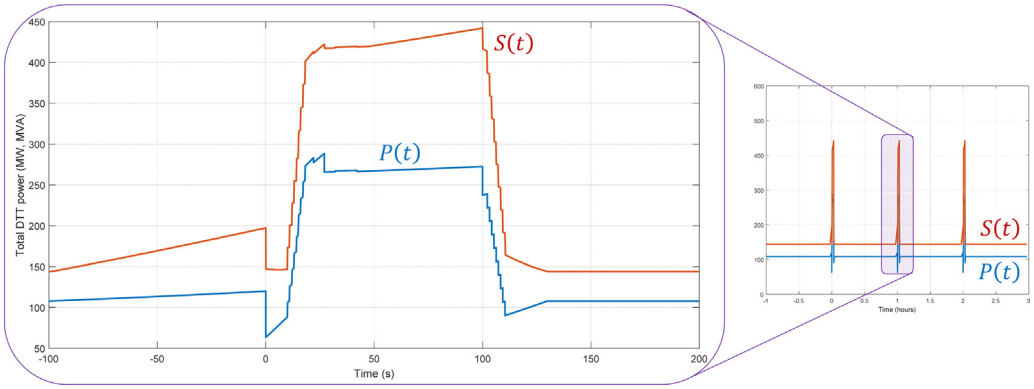

Fig. 11. Total electrical powers of the DTT facility for the reference scenario. The plot on the left is the zoom of a single experiment taken from the plot on the right showing three consecutive experiments at the nominal duty cycle (100s/3600s).

to 130 MW. A similar progressive reduction is expected in the discharge phase.

5. Auxiliary power supplies

Several auxiliary systems and services are necessary for the DTT operations [2–7]: fueling, vacuum systems, pumps, cooling and cryogenic systems, diagnostics, control and monitoring, remote handling, compressed air and fluid services, communication interfaces, computers, air conditioning and so on.

The contribution from the auxiliary systems was estimated assuming a constant power demand of 90 MW with $\cos\varphi = 0.75$. This model takes into account also the TFC contributions.

Fig. 10 summarizes the models assumed for the estimation of the contributions due to the additional and auxiliary powers.

6. DTT power scenarios

Fig. 11 shows the total active and apparent powers resulting from all the contributions described in the previous sections. In order to ensure a good safety margin, a 20% increment was applied on both the estimated active and the reactive powers, so obtaining the power time evolutions in Fig. 11.

It is important to stress that the plant is designed to operate at these power levels with the nominal duty cycle of 100s/3600s. Most of the experimental campaigns, especially in the first months of operations, are expected to be performed at reduced power with shorter times.

Extending the results for a single scenario, Fig. 11 shows the power profiles for more consecutive experiments during a working day. Since this is a good model of the most demanding load affecting the national grid, it was submitted to the Italian national grid operator (TERNA) for the required analyses and authorizations (see Section 8.1).

Of course, in order to provide a general overview of the situation, the graphs include the reactive powers before any intervention for power factor correction. This topic is addressed in Section 8.2.

7. Preliminary ratings of PS components

The previous analyses were useful also to identify the preliminary characteristics of the main DTT PS systems and components. Even though further optimization will be possible, an effort was performed to obtain homogenous or modular structures for cost reduction and maintenance simplification. This is summarized by the bars in Fig. 12 and in Fig. 13.

All the Base PSs were designed to operate on 4 quadrants, being able to produce both forward and backward currents, even when

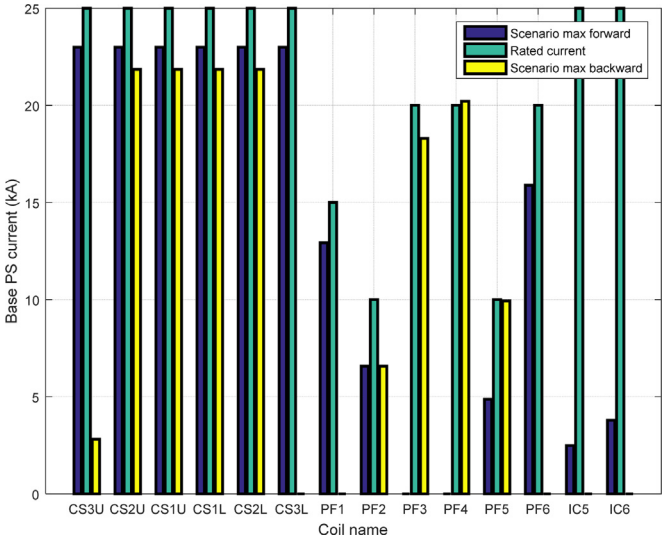

Fig. 12. Comparison between the Base PS rated currents and the values reached in the reference scenario.

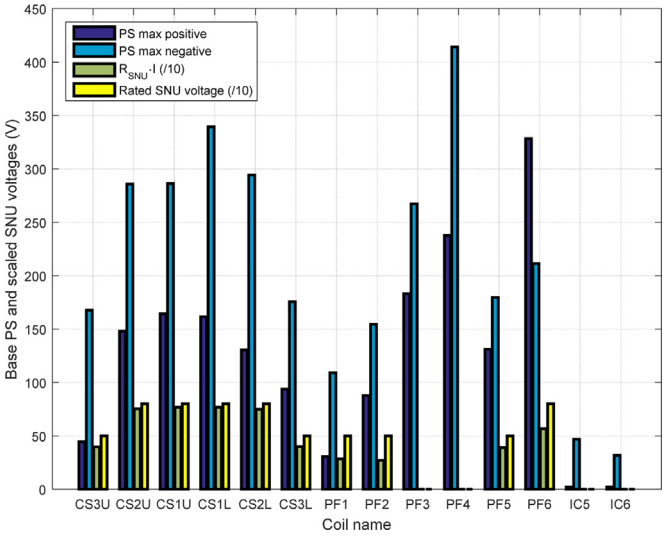

Fig. 13. Voltage reached in the reference scenario by the Base PSs and SNUs compared with the rated SNU voltages (the SNU voltages are scaled for visualization purposes). The coils PF3, PF4, IC5 and IC6 have no SNUs.

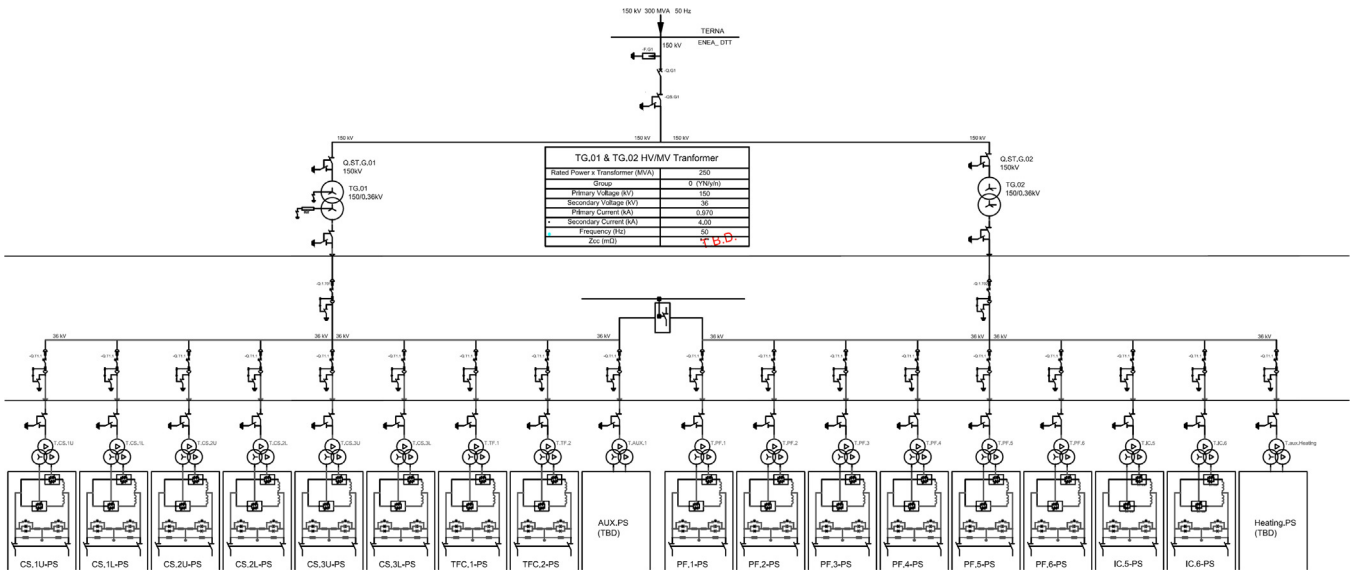

Fig. 14. Preliminary scheme of the DTT electrical distribution and PS system.

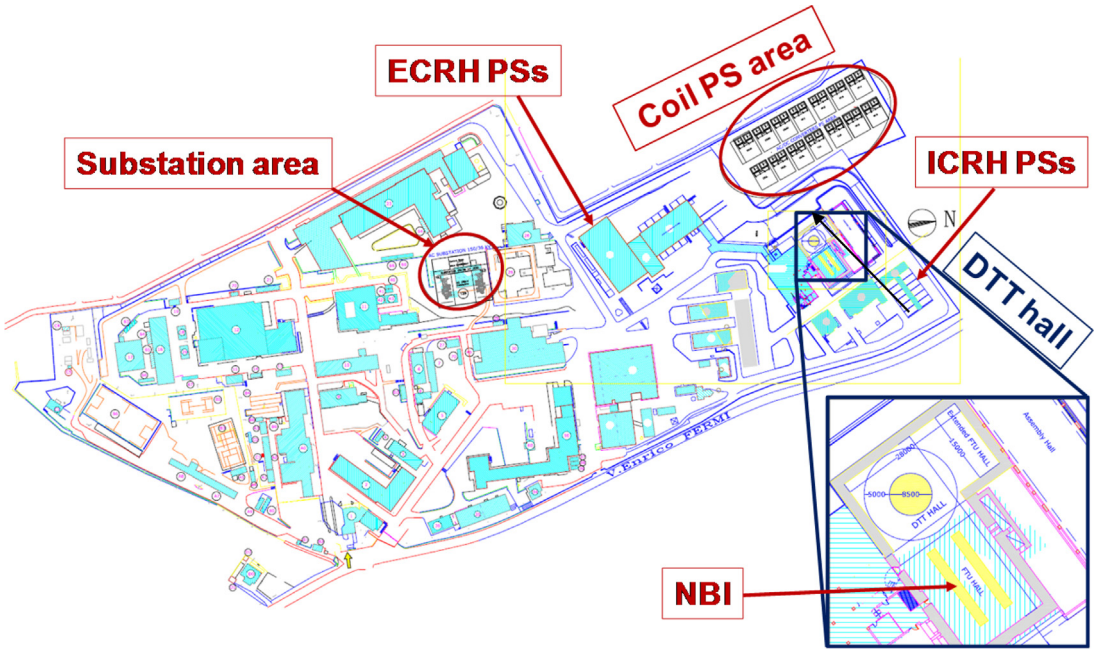

Fig. 15. Map of the Frascati Research Center with emphasis on the main modification for the installation of the DTT electrical facilities.

it was not strictly required by the available scenarios (see also Fig. 3). The output current and voltage ratings were mostly divided in classes of ±15 kA, ±20 kA and ±25 kA, to be implemented by modular 5 kA bridges in parallel.

Except for IC5 and IC6, all the Base PSs are based on 12-pulses self-commutated (thyristor) bridges with circulating current. The expected voltage rating is ±800 V. The IC5 and IC6 PSs are based on IGBT or IGCT devices with ±1 kV output voltage to be fast enough to control the plasma vertical position and to cover a wide range of situations.

The DTT PSs will be directly connected to the national grid (see Section 8), differently from the present ENEA tokamak (FTU) that is mostly supplied through flywheels. This would result in a very stable frequency (50 Hz), reducing the modelling and design problems due to the variable frequency.

Since the SNU resistance values obtained from the calculations introduced in Section 2.4 are quite homogenous and well implementable (similar to those built for JT-60SA [15]), they were used to calculate the voltages produced across the SNU for the current actually flowing at the breakdown. These voltages are compared in Fig. 13 with the SNU nominal voltages. Furthermore, several possible resistance combinations will be available in the final design. In the final design, the voltages of all the ten SNUs have to rise quickly and with a jitter that is much shorter than 1 ms (that is compatible with the experimental results of the JT-60SA SNUs [20]).

Thanks also to the polarity changer, the TFC Base PS can be rated to operate at maximum 50 kA on two quadrants with 12 pulses.

The performances in Table 1 can be achieved by high voltage PSs based on IGBTs or MOSFETs and controlled by pulse step modulation [12,13]. In this case, transformers with multiple secondary windings implement the connection to the medium voltage grid.

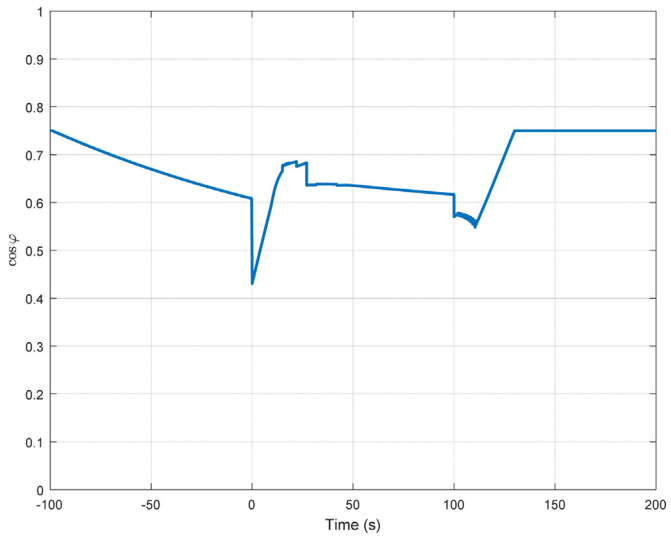

Fig. 16. Instantaneous power factor of the entire DTT plant during the reference scenario.

As mentioned in the Introduction, all the design choices and selected technologies are expected to be feasible in the available time, even though some of them should reach extremely high performances. However, it is worth noticing that some improvements are under consideration, as for the SNUs and the FDUs, whose functions could be unified. Furthermore, an alternative approach based on supercapacitors [24] is being investigated especially for the fast PSs as for IC5 and IC6.

8. Electrical distribution system

The ENEA Research Center located in Frascati (close to Rome) is the main candidate as DTT site. This section presents the systems to transmit the electrical power to the Center and to distribute it to the DTT loads.

8.1. Possible connection to the Italian national grid

A new connection to the national extra high voltage (EHV) grid at 400 kV has been foreseen [10] by an intermediate dedicated electric substation 400 kV/150 kV in proximity to an important node with adequate power. This is also the border of the ENEA property and responsibility. Two underground electric cables would connect the 400 kV/150 kV substation to another substation 150 kV/36 kV inside the ENEA Research Center.

Fig. 14 shows a simplified scheme of the DTT PS and electrical distribution systems, considering a 150 kV/36 kV substation with two 250 MVA transformers. The double path for both the high voltage cables and the substation transformers should ensure a high level of redundancy and reliability. However, the final technical choices are still under discussion.

The map in Fig. 15 shows the main modifications to the ENEA Research Center in Frascati foreseen to upgrade the electrical facilities for DTT. In particular, the electric substation, the converter area and the tokamak building (modified from the FTU hall) are emphasized. The involved areas have been identified, considering the overall dimensions of each electrical device.

8.2. Power factor correction and harmonics limitation

The power factor during the 100 s operation is shown in Fig. 16.

According to the Italian Grid Code, the maximum allowable power factor is 0.75. The target of the DTT design is to continuously correct the power factor to 0.9. The reactive power that has to be compensated is about 220 MVar. The apparent power peak seen by the national grid is expected to be about 350 MVA.

This could be achieved either by a centralized or by distributed systems. The former solution could use specific static VAR compensators [25] or exploit the existing FTU motor flywheel generator MFG3 rated 250 MVA. The main contribution to the latter solution consists in the introduction of a sequential control in the thyristor bridges [17,26]. The choice among these options is mainly based on economic evaluations.

Some filters will be inserted before the connection to the EHV grid, though the harmonic content is not expected to be excessive thanks to the 12-pulse operations.

9. Conclusions

The DTT facility aims to study the power exhaust problem for future experiments and reactors. This requires a complete tokamak with a comprehensive set of PS systems, including at least 30 superconducting coils, about 120 MW for the additional heating systems and almost 100 MW for the auxiliary services.

The voltages, currents and powers to be provided by the PSs were estimated moving from a reference scenario and introducing a reasonable safety margin also to allow modifications and future upgrades. Using these data, the preliminary characteristics of some relevant PS components were identified.

The feasibility of the DTT scenarios at the ENEA Center in Frascati was verified, including a continuous correction of the power factor up to 0.9. The solution identified to supply all the facility directly from the national grid requires the installation of a new 150 kV cable line specifically for DTT and a new substation with two 150 kV/36 kV transformers inside the ENEA Center.

The independent evaluation of the electrical requirements of each PS system led to the definition of the active, reactive and apparent power scenarios. Due to the pulsed PSs (serving CS, PFC, IC, ECRH, ICRH, NBI), the 100-MVA permanent load can exceed 400 MVA with a duty cycle of 100s/3600s, but the power factor correction should reduce to 350 MVA the maximum request from the national grid.

Acknowledgement

This work has been carried out within the framework of the EUROfusion Consortium and has received funding from the Euratom research and training programme 2014–2018 under grant agreement No 633053. The views and opinions expressed herein do not necessarily reflect those of the European Commission.

References

[1] EFDA, Fusion Electricity—A roadmap to the realisation of fusion energy, November 2012, 2012, Online: http://users.euro-fusion.org/iterphysicswiki/images/9/9b/EFDA_Fusion_Roadmap_2M8JBG_v1_0. pdf.
[2] G. Rostagni, The electric power handling from present machines to fusion power stations, Fusion Eng. Des. 74 (1–4) (2005) 87–95.
[3] L. Novello, et al., Advancement on the procurement of power supply systems for JT-60SA, in: IEEE 25th Symposium On Fusion Engineering (SOFE), Austin, Texas, USA May 31–June 4, 2015.
[4] J. Hourtoule, et al., ITER electrical distribution system, in: IEEE 25th Symposium on Fusion Engineering (SOFE), San Francisco, CA, 2013, pp. 1–5.
[5] S. Nair, J. Hourtoule, K.W. Kang, J. Journeaux, M. Khedekar, Instrumentation and control of the ITER electrical power distribution system, Electr. Mach. Syst. (ICEMS) (2013).
[6] C. Neumeyer, et al., ITER power supply innovations and advances, in: IEEE 25th Symposium on Fusion Engineering (SOFE), San Francisco, CA, 2013, pp. 1–8.
[7] M. Matsukawa, Engineering feature in the design of JT-60SA, Proc. of the 21 Fusion Energy 2006, IAEA Conference (2007).
[8] F. Crisanti, et al., The DTT device: rationale for the choice of the parameters, Fusion Eng. Des. (2017), Special Issue for DTT.

[9] R. Ambrosino, et al., The DTT device: poloidal field coil assessment for alternative plasma configurations, Fusion Eng. Des. (2017), Special Issue for DTT.
[10] R. Martone, et al., The DTT device: costs and management aspects, Fusion Eng. Des. (2017), Special Issue for DTT.
[11] A. Di Zenobio, et al., The DTT device: conceptual design of the superconducting magnet system, Fusion Eng. Des. (2017), Special Issue for DTT.
[12] G. Granucci, et al., The DTT device: systems for heating, Fusion Eng. Des. (2017), Special Issue for DTT.
[13] P. Zito, et al., A novel conceptual design for gyrotron's high voltage power supplies, in: 42nd IEEE Industrial Electronics Conference (IEEE IECON2016), Florence Italy, 2016.
[14] L. Zanotto, A. Maistrello, L. Novello, V. Toigo, Impact of consorzio RFX facilities for thermonuclear fusion research on the italian extra high voltage network harmonics and quality of power (ICHQP), in: IEEE 15th International Conference on, Hong Kong, 2012, pp. 605–611.
[15] A. Lampasi, A. Coletti, L. Novello, M. Matsukawa, F. Burini, G. Taddia, et al., Final design of the switching network units for the JT-60SA central solenoid, Fusion Eng. Des. 89 (2014) 342–348.
[16] E. Gaio, A. Ferro, L. Novello, M. Matsukawa, Power amplifiers based on SiC technology for MHD mode control in fusion experiments, IEEE Trans. Plasma Sci. 99 (2017) 1–8.
[17] P., Zito, D.A., Lampasi, G., Maffia, G., Candela, A Novel Digital Controller for 12-Pulse Back-to-Back AC/DC Converters in Nuclear Fusion Experiments, International Symposium on Power Electronics, Electrical Drives, Automation and Motion (SPEEDAM 2014), Ischia, Italy, 18–20 Jun. 2014.
[18] P. Zito, et al., Design and realization of JT-60SA fast plasma position control (FPPC) power supplies, Fusion Eng. Des. 98–99 (2015) 1191–1196.
[19] A. Maistrello, et al., Experimental qualification of the hybrid circuit breaker developed for JT-60SA quench protection circuits, IEEE Trans. Appl. Supercond. 24 (3) (2014).
[20] A. Lampasi, et al., First switching network unit for the JT-60SA superconducting central solenoid, Fusion Eng. Des. 98–99 (2015) 1098–1102.
[21] G. Moltgen, Converter Engineering. An Introduction to Operation and Theory, Siemens John Wiley and Sons, 1984.
[22] A. Kloss, A Basic Guide to Power Electronics, John Wiley and Sons, 1984.
[23] L. Novello, et al., Analysis of maximum voltage transient of JT-60SA toroidal field coils in case of fast discharge, IEEE Trans. Appl. Supercond. 26 (no. 2) (2016) 1–7.
[24] A. Lampasi, G. Maffia, G. Taddia, S. Tenconi, P. Zito, ETHICAL: a modular supercapacitor-based power amplifier for high-current arbitrary generation, Florence, Italy, in: 16th IEEE International Conference on Environment and Electrical Engineering (EEEIC), 7–10, 2016.
[25] C. Finotti, E. Gaio, I. Song, J. Tao, I. Benfatto, Improvement of the dynamic response of the ITER reactive power compensation system, Fusion Eng. Des. 98–99 (2015) 1058–1062.
[26] K. Shimada, et al., Minimization of reactive power fluctuation in JT-60SA magnet power supply, Plasma Sci. Technol. 15 (February (2)) (2013).